Results in Physics 14 (2019) 102366

Contents lists available at ScienceDirect

Results in Physics

journal homepage: www.elsevier.com/locate/rinp

Superparamagnetic iron oxide nanoparticles for full-color photonic materials with tunable properties

Wei Wang[a,b], Qianli Li[c], Ang Zheng[a,b], Xiaolei Li[c], Zeyu Pan[a], Jinchun Jiang[a], Linquan Zhang[a], Ruijiang Hong[a,*], Lin Zhuang[a,*]

[a] Institute for Solar Energy Systems, Guangdong Provincial Key Laboratory of Photovoltaics Technologies, School of Physics, Sun Yat-sen University, Guangzhou 510006, People's Republic of China
[b] School of Materials Science and Engineering, Sun Yat-sen University, Guangzhou 510006, People's Republic of China
[c] Department of Orthodontics, Guanghua School of Stomatology, Hospital of Stomatology, Guangdong Provincial Key Laboratory of Stomatology, Sun Yat-sen University, Guangzhou 510055, People's Republic of China

ARTICLE INFO

Keywords:
Photonic materials
Nanostructure
Superparamagnetic nanoparticles
Structural color

ABSTRACT

To obtain full-color tunable photonic materials, superparamagnetic nanoparticles with a tunable particle diameter and highly charged surfaces were synthesized through a modified solvothermal process. Compared with polyelectrolyte-capped nanoparticles, citrate-capped nanoparticles are simple, cost-effective, and suitable as building blocks of tunable photonic materials. The reflection spectra of superparamagnetic colloid under a varing magnetic field covers a broad wavelength range of approximately 420–820 nm due to the assembly of Fe_3O_4 nanoparticles. The effect of the optical properties of colloids on variables such as the nanoparticle size, nanoparticle concentration, ionic strength, and pH value was studied. After superparamagnetic Fe_3O_4 nanoparticle was coated with a layer of silicon dioxide, their reflection spectra covered the electromagnetic range from the visible to near-infrared region. Superparamagnetic colloids can produce structural colors with engineered nanostructures, which indicates that citrate-capped Fe_3O_4 nanoparticles and Fe_3O_4@SiO_2 core-shell nanoparticles as photonic materials are promising candidates for achieving full-color display.

Introduction

Magnetic nanoparticles have been widely used in broad technological applications, including bioseparation [1–3], catalysts [4–6], displays [7–9], and energy storage [10], because of their intrinsic magnetic properties, nanometer size, and surface morphology. Among the various magnetic particles, iron oxide (Fe_3O_4) nanoparticles are considered a potential candidate for scientific research due to their unique magnetic features and self-assembly property. Various methods, such as chemical co-precipitation [11–13], thermal-decomposition method [14–16], solvothermal method [17–19], and hot injection [20–22], have been developed to produce magnetic Fe_3O_4 nanocrystals. Generally, by adjusting the lattice between the nanoparticles, artificial photonic materials can be modulated to produce tunable structural color [23,24]. Superparamagnetic Fe_3O_4 show its special application in photonic materials in an external magnetic field, which display structural color, an optical phenomenon, that have widely used in broad technological applications, such as sensors [25], smart windows [26], catalysts [27], displays [28], and textiles [29].

Various polyelectrolytes have recently been used to synthesize Fe_3O_4 for controlling superparamagnetic colloid preparation, wherein these polyelectrolyte-capped nanoparticles act as building blocks of tunable photonic materials. Yin et al. explored poly(acrylic acid)-capped Fe_3O_4 monodisperse nanoparticles with superparamagnetic property and exhibiting rapidly optical responses and that reported that this process requires complicated synthesis conditions [30]. Guan et al. synthesized superparamagnetic Fe_3O_4@PVP particles by adding dextrose and poly-vinylpolypyrrolidone; these particles could provide a multicolor display, but not including violet wavelengths [31]. Asher et al. developed monodisperse superparamagnetic colloidal spheres to reflect limited visible light under a magnetic field, but their reflection peaks were easily affected by electrolyte concentration [32]. Polyelectrolyte-capped Fe_3O_4 nanoparticles dispersed in aqueous solution can be employed in photonic materials with engineered nanostructures by using an external field; however, their limitations include complicated synthesis conditions, limited structural colors, and low stability of structural colors in complex environments.

Sodium citrate (Na_3Cit), a small molecular modifier containing

* Corresponding authors.
E-mail addresses: hongruij@mail.sysu.edu.cn (R. Hong), stszhl@mail.sysu.edu.cn (L. Zhuang).

https://doi.org/10.1016/j.rinp.2019.102366
Received 13 February 2019; Received in revised form 3 May 2019; Accepted 20 May 2019
Available online 24 May 2019
2211-3797/ © 2019 The Authors. Published by Elsevier B.V. This is an open access article under the CC BY-NC-ND license (http://creativecommons.org/licenses/BY-NC-ND/4.0/).

three carboxylate groups, is widely used as a stabilizer for the modification of various nanocrystals [33–36]. As a strong base–weak acid salt, Na_3Cit has a strong buffer capacity, thermal stability, and low impact on the environment. Na_3Cit is also employed as an ideal surfactant for inorganic particles [37–39]. However, few reports exist on the use of Na_3Cit as a stabilizer to exhibit structural colors with an external field response. In addition, core–shell nanoparticle has attracted much attention in the past decade, because they possess unique optical properties and have better chemical stability than nanoparticles without coating shell. In particular, coating a SiO_2 layer on the particle surface increases the nanoparticle diameter; this overcomes the limitation of the solvothermal method, wherein iron oxide nanoparticles with diameters of only $\leq$150 nm are synthesized [31,38]. Besides, Fe_3O_4@SiO_2 also show the potential being the artificial photonic materials for its uniform sphere and quick magnetic response, even in different solvents, including aqueous solutions, ethylene glycol, and polymers [7,40,41]. Moreover, it prevents the release of ions and detachment of the stabilizer, which improves the chemical stability of nanoparticles.

Hence, a modified solvothermal process was employed to prepare superparamagnetic Fe_3O_4 nanoparticles with a tunable size and highly charged surfaces. Throughout the high-temperature reaction, citrate-capped nanoparticles retained their thermodynamic stability and hydrophilicity. Because of the controlled nanoparticles diameter, colloid concentration, and magnetic field, the range of reflection spectrum of photonic materials is wide across the visible region. Even with high electrolyte (NaCl) concentration, the colloids remained stable and produced structural colors. The aforementioned properties indicate that superparamagnetic nanoparticles can be used as building blocks to achieve tunable structural colors with engineered nanostructures. Moreover, we study the particles after being coated with SiO_2, thanks to its larger nanoparticle diameter, whose reflection spectrum appears in near-IR regions under the magnetic field. The synthesized superparamagnetic nanoparticles, exhibiting excellent performance of structural colors, are promising candidates for achieving full-color display; they can also aid in understanding the mechanisms of photonic materials.

Experimental

Characterization

The magnetic property (M-H curves) at indoor temperature was examined using a Lakeshore 7404 vibrating sample magnetometer. The X-ray diffraction (XRD) pattern was obtained using an Empyrean diffractometer with Cu Kα radiation. The infrared spectrum was recorded using a Tensor-27 Bruker Fourier transform infrared (FT-IR) spectrometer. The structural color of the photonic materials built by the nanoparticles with a magnetic field was observed using a PG4000 optic fiber spectrometer (Ideaoptics) coupled to a 6-around-1 reflection/backscattering probe. The zeta potential of Fe_3O_4 colloids were determined using a Nano ZS-90 Zetasizer (Marlvern, England). The X-ray photoelectron spectroscopy (XPS) pattern was determined using a Thermo-VG Scientific ESCALAB 250 XPS photoelectron spectrometer. The morphology and diameter of the nanoparticle was observed on a JEM-2100F transmission electron microscope.

Preparation of Fe_3O_4 and Fe_3O_4@SiO_2 colloids

Iron oxide nanoparticle was obtained using a modified solvothermal process. In the synthesis process, 1.7 g of iron chloride hexahydrate and 0.06 g of ferrous chloride tetrahydrate were dissolved in 30 mL of diethylene glycol (DEG). 30 mL of ethylene glycol (EG) was prepared, which contained 1.6 g of polyethylene glycol (PEG), 0.64 g of sodium citrate (Na_3Cit), and 3.0 g of sodium acetate dihydrate. The average sizes of iron oxide nanoparticles were under the control of the mass ratio of Na_3Cit/NaOAc. The two as-prepared mixtures were mixed and then transferred to a Teflon-lined stainless steel autoclave. In electrically heated drying oven, the dark solution was then heated to 220 °C for 360 min. The iron oxide nanoparticle was thoroughly washed with ethyl alcohol and deionized H_2O and then dispersed in various amounts of deionized H_2O to obtain Fe_3O_4@SiO_2 colloids with different concentrations.

Fe_3O_4@SiO_2 nanoparticle was prepared using a modified Stöber method. In the coating process, 12 mL of deionized H_2O was added to a mixture of 80 mL ethanol and 8 mL ammonia. Then, 100 mg of Fe_3O_4 nanoparticles was added to the as-prepared solution. This as-prepared solution was added to a flask and experienced to high speed stirring at 55 °C for 30 min for forming a well-mixed colloid. Then, tetraethyl orthosilicate (TEOS) was mixed quickly to the colloid every 0.5 h. After the reaction, the as-obtained solution was sedimented through centrifugation at 12,000 rpm for 20 min. After all the impurities were removed, deionized water was added and the core–shell nanoparticle was redispersed through ultrasonication.

The formation process for full-color photonic materials

After additional small molecular modifiers are removed through magnetic separation with ethanol and deionized water, superparamagnetic nanoparticles can assemble to as photonic materials in deionized water through the application of a magnetic field. When a circular magnet is slowly moved toward the colloids in a cuvette, the behave of colloid change from Brown fuild to orderly photonic structure. The interparticle spacing of photonic structure can be adjusted by the external magnetic field. If the magnetic field strength is maintained, one color is observed in the reflectance spectrum with optic fiber spectrometer.

Results and discussion

To construct full-color tunable photonic materials, superparamagnetic and citrate-capped Fe_3O_4 nanoparticles were first synthesized as building blocks. During the reaction, ferric ions were partly reduced in a mixture of EG and DEG. The mixture contained both low-molecular-weight sodium citrate and high-molecular-weight PEG. As depicted in Fig. 1a, the as-obtained Fe_3O_4 nanoparticles had a spherical shape and an almost uniform particle diameter. The average diameter of the Fe_3O_4 nanoparticles was approximately 135 nm. The selected area electron diffraction pattern exhibited spotty diffraction rings, which indicated the polycrystalline structure of the nanoparticles (Fig. 1b). As depicted in the high-resolution transmission electron microscopy (HRTEM) image of the Fe_3O_4 nanoparticles, the interfringe spacing (0.46 nm) was close to the interplane distance of the (1 1 1) lattice planes in the face-centered cubic Fe_3O_4 (Fig. 1c). Fig. 1d indicates that the core–shell nanoparticles had an inorganic Fe_3O_4 core and a silicon dioxide shell of approximately 50 nm.

The powder XRD pattern for the three Fe_3O_4 nanoparticle sizes is displayed in Fig. 2a, which confirms the crystalline nature of the magnetic nanoparticles. The average size of the primary nanocrystals (approximately 8–12 nm) was calculated by considering the strongest peak, which is assigned to the (3 1 1) plane, and applying the Debye–Scherrer equation. The calculation result suggested that the Fe_3O_4 nanoparticles had a double-stage hierarchical structure, which is in agreement with the HRTEM result. The diffraction peaks appeared from 15° to 80° are associated to the (2 2 0), (3 1 1), (4 0 0), (4 2 2), (5 1 1), and (4 4 0) planes of iron oxide nanocrystal with an inverse spinel structure (JCPDS No. 75-0033). To study the magnetic properties of the Fe_3O_4 core, its mass magnetizations were characterized by applying a magnetic field of −12,500 to 12,500 G at 300 K. As displayed in Fig. 2b, the saturation magnetization (Ms) values of the 71, 100, and 135 nm Fe_3O_4 nanoparticles were 59.6, 66.2, and 70.4 emu/g, respectively. The Ms values of the Fe_3O_4@SiO_2 coated with silicon dioxide of

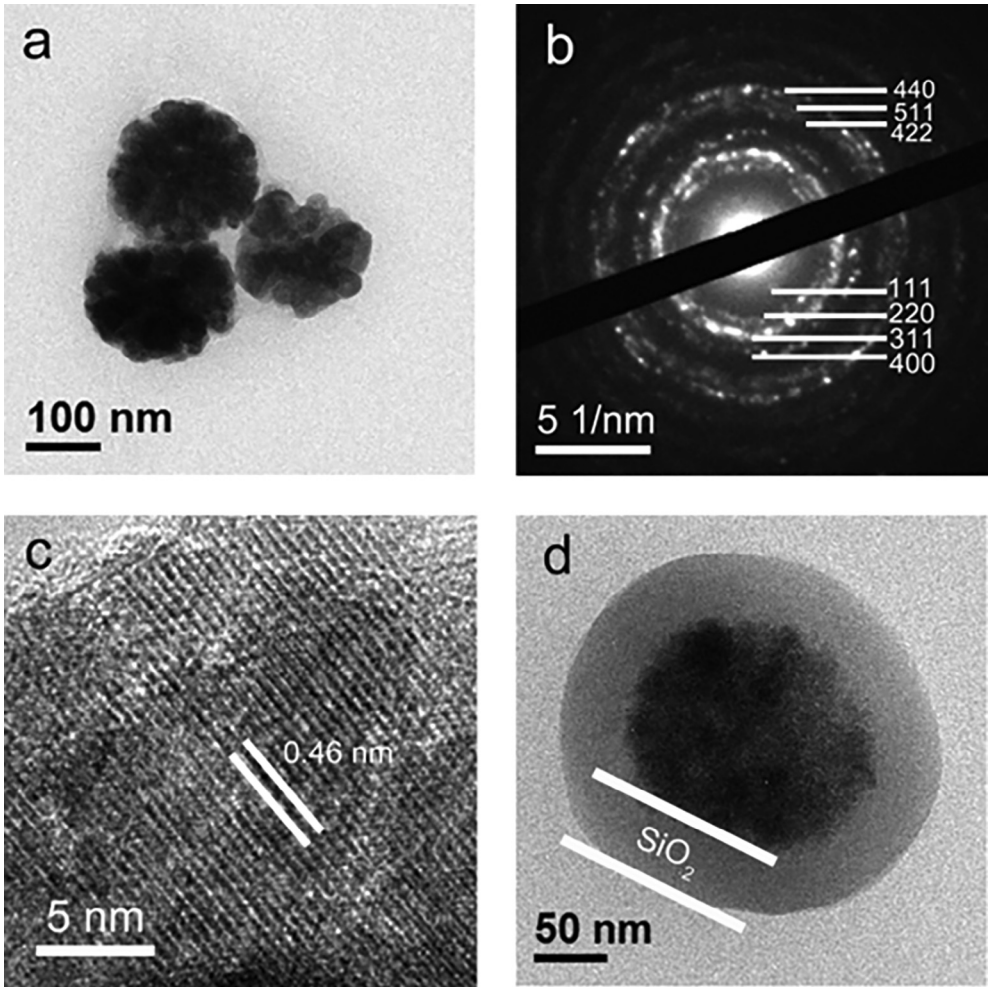

Fig. 1. (a) Transmission electron microscopy (TEM) image of Fe_3O_4 nanoparticles; (b) selected area electron diffraction image of a Fe_3O_4 nanoparticle; (c) high-resolution TEM (HRTEM) image of a single Fe_3O_4 nanoparticle; and (d) TEM image of core–shell Fe_3O_4@SiO_2 nanoparticles.

different thicknesses with the same Fe_3O_4 core size (100 nm) were 43.3 (10-nm shell), 32.3 (25-nm shell), and 13.8 (50-nm shell) emu/g, respectively. Because the diameter of the primary nanocrystals does not exceed that of a magnetic domain (approximately 30 nm), the samples with inappreciable coercive force and remanent magnetization exhibited superparamagnetism at an indoor temperature. After coating SiO_2 on the shell, the Ms values in core-shell nanoparticles decreased and still exhibited superparamagnetism. The superparamagnetism assisted the rapid assembly of magnetic nanoparticles into a nanostructure. The presence of citrate groups and SiO_2 shells was confirmed through FT-IR spectroscopy (Fig. 2c). The bands at 580 cm^{-1} corresponded to the iron oxide band stretching vibration of the Fe_3O_4 nanoparticles, and the bands at 1382 and 1591 cm^{-1} were attributed to the −C═O− component. In contrast to Fe_3O_4 without $NaCit_3$ (yellow line), the citrate-capped Fe_3O_4 (blue line) had a band of citrate groups. The two bands of Fe_3O_4@SiO_2 with red lines at 942 and 1071 cm^{-1} corresponded to the bending vibrations of Si-OH and SiO_2 shells, respectively, which suggested the generation of asymmetric stretching vibrations between the siloxane bonds. Both citrate groups and SiO_2 shells provided the Fe_3O_4 nanoparticles with high water solubility for constructing full-color tunable photonic materials. For the Fe_3O_4 nanoparticles displayed in Fig. 2d, the deconvolution of the Fe 2p spectra produced octahedral Fe^{2+} (Fe^{2+}(Oct)), octahedral Fe^{3+} (Fe^{3+}(Oct)), and tetrahedral Fe^{3+} (Fe^{3+}(Tet)) peaks, which exhibited magnitudes of 709.7, 710.8, and 712.7 eV, respectively. Moreover, the area ratio of Fe^{3+}/Fe^{2+} was approximately 2.3, which is in agreement with the stoichiometric results of Fe_3O_4. The aforementioned values were in agreement with the previously reported Fe 2p XPS spectrum for iron oxide nanoparticles [42–44]. For the citrate-capped Fe_3O_4, carboxyl groups could be observed in the XPS O 1s and C 1s regions, as depicted in Fig. 2e and f. Their binding energy was assigned to data in references for citrate-capped Fe_3O_4 [45,46]. The peaks of O 1s XPS spectra (Fig. 2e) at 531.3 and 530.0 eV were assigned to C−O and lattice O, respectively. The C 1s XPS spectra (Fig. 2f) with binding energies at 284.9, 286.7, and 288.5 eV corresponded to C−C, C═O, and O═C−O, respectively. As depicted in Fig. S1, both C 1s and O 1s were observed on citrate-capped Fe_3O_4 nanoparticles and Fe_3O_4@SiO_2 nanoparticles. These results indicated that the citrate was chemically bonded to the surface of the Fe_3O_4, which concurred with the FT-IR results.

Compared with polyelectrolyte-capped Fe_3O_4 nanoparticles [47,48], our samples exhibited higher quality magnetism performance, which was obtained using citrate groups as a stabilizer and high-boiling-point DEG as the solvent. Moreover, the obtained Fe_3O_4 had a high yield (260 mg/batch) and saturation magnetization even when pure Fe_3O_4 was separated from the reaction products. Thus, Fe_3O_4 nanoparticles have considerable potential in mass production for industrial uses.

After additional small molecular modifiers are removed through magnetic separation with ethanol and deionized water, superparamagnetic nanoparticles can assemble to as photonic materials in deionized water through the application of a magnetic field (H). In the absence of an external H, the superparamagnetic colloids appear a classical brown ferrofluid, and the structural color of colloids appear black (Fig. 3a, left). However, when a H is applied to Fe_3O_4 colloids, the

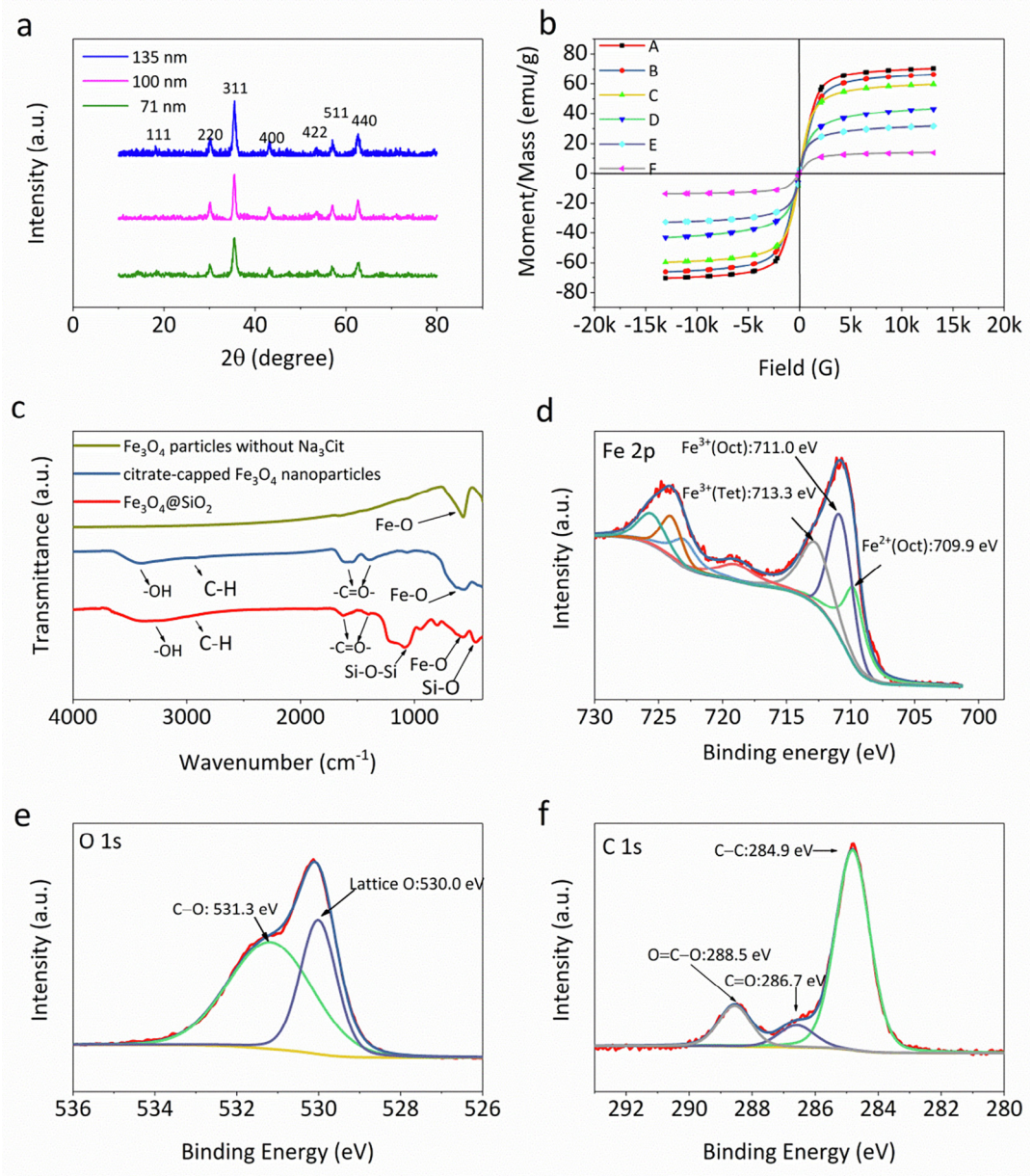

Fig. 2. (a) XRD patterns of Fe_3O_4 nanoparticles having a size of 71, 100, and 135 nm; (b) magnetization curve of Fe_3O_4 nanoparticles having a size of 71 (A), 100 (B), and 135 nm (C) and Fe_3O_4@SiO_2 nanoparticles having the same core size 100 nm with 10 (D), 25 (E), 50 nm (F) SiO_2 shell at room temperature; (c) FT-IR spectra of Fe_3O_4 nanoparticles without Na_3Cit, citrate-capped Fe_3O_4 nanoparticles, and Fe_3O_4@SiO_2 nanoparticles; XPS spectrum of Fe_3O_4 with curve fitting for (d) Fe 2p, (e) O 1s, and (f) C 1s photoelectron region profiles.

structural color of colloids immediately changes (Fig. 3a, right). For example, when a circular magnet is slowly moved toward the colloids in a cuvette, the colloid demonstrate several colors (Fig. 3b). If the magnetic field strength is maintained, one color is observed in the reflectance spectrum with single peak. Thus, under an external magnetic field, an orderly photonic structure forms.

The Fe_3O_4 nanoparticles were well dispersed in water due to their highly charged surface. The establishment of a balance between the magnetic packing forces and electrostatic repulsive forces contributed to the magnetic assembly of the Fe_3O_4 nanoparticles. The electrostatic repulsive force is an interaction force provided by the citrate group from iron oxide nanoparticles. The magnetic packing force is also an interaction force, explained as $Fm = \nabla (\mu H)$, where μ represents the magnetic moment and H the applied magnetic field [49,50]. In the direction perpendicular to the magnetic field, the particles maintain their spacing by electrostatic repulsive forces. When a magnetic field is applied to the colloids, interaction forces, including the electrostatic-repulsive and magnetic-packing forces, develop between adjacent nanoparticles, thereby forming the photonic material structure. Several nanoparticles first assemble to form a chainlike nanostructure because of the balance of electrostatic-repulsive and magnetic-packing forces, which is typical for magnetic colloid particles [51–53]. All chainlike nanostructures along the direction of the magnetic field further assembled into three-dimensional structures to produce structural colors at a certain concentration. The electrostatic-repulsive forces could be used to balance the magnetic-packing forces to create 3D structures with tunable interparticle spacing, resulting in widely tunable reflectance that can be changed by applying a varying magnetic field. Because all forces were isotropic and the nanoparticles were spheres, the 3D photonic crystals were created when the external magnetic field was applied to the colloids. The 3D photonic crystals exhibited periodical interparticle spacing in the 160–320-nm range in accordance

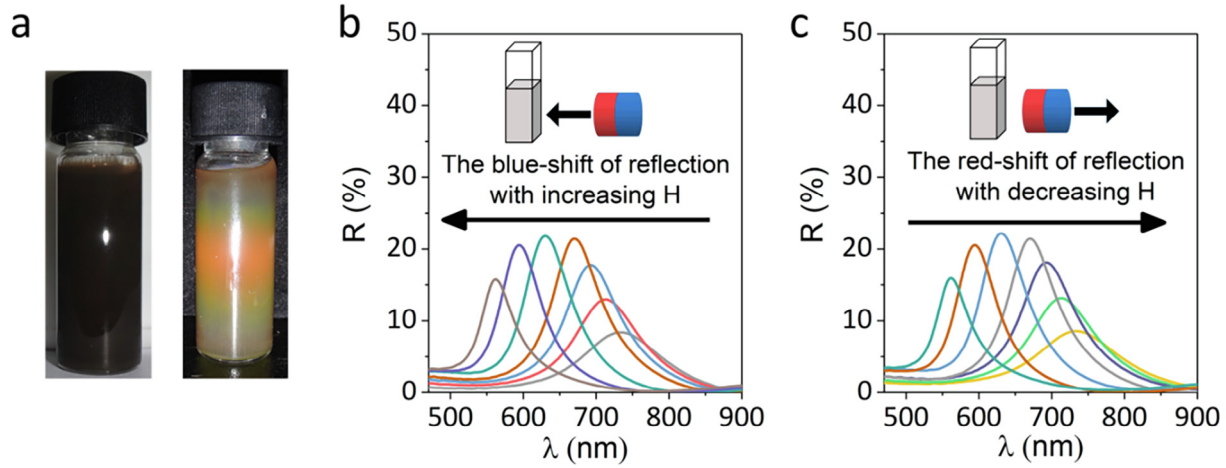

Fig. 3. Reversible optical responses of a 100 nm Fe_3O_4 colloid under increasing or decreasing external magnetic field (H): (a) digital photos of the Fe_3O_4 colloid without H (left) and with H (right); (b) blue shift in the reflection when H is enhanced; and (c) red shift in the reflection when H is weakened. (For interpretation of the references to color in this figure legend, the reader is referred to the web version of this article.)

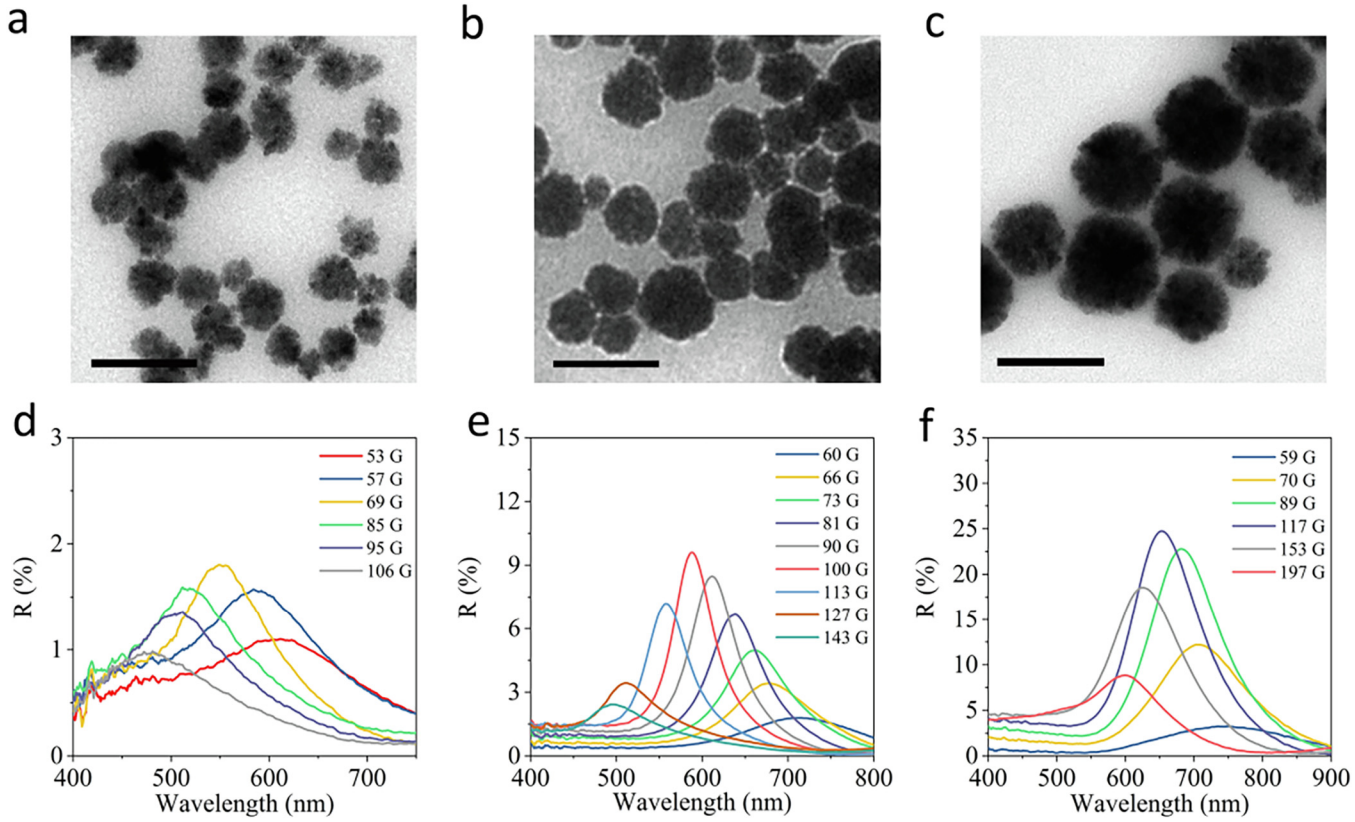

Fig. 4. TEM images indicating the influence of the particle diameter on the shift range of the reflection peaks. The average size of the superparamagnetic nanoparticles in (a–c) was 71, 100, and 135 nm, respectively. The scale bars in (a–c) correspond to 100 nm. For each colloid, the reflection peaks exhibit a blue shift when H increases from (a) 44 to 106 G, (b) 55 to 143 G, and (c) 59 to 197 G. (For interpretation of the references to color in this figure legend, the reader is referred to the web version of this article.)

with Bragg's Law; this range represents the basic photonic unit for the diffraction of electromagnetic waves.

The reflection wavelengths could be tuned by changing the strength of the magnetic field and changing the distance between the colloids and magnet (inset of Fig. 3b,c). The Fe_3O_4 colloids produced reversible structural colors under a varying magnetic field (H). When the distance between the colloids and magnet was decreased, the local H increased from 40 to 150 G and the reflection wavelengths exhibited a blue shift from 860 to 500 nm. As evident in Fig. 3b, the reflection wavelengths of the colloids were gradually blue-shifted when H increased. By contrast, when H decreased, the reflection peaks of the sample exhibited a red shift (Fig. 3c). The colloids maintained a stable state in the changing magnetic field. However, nanoparticle deposition occurred when the colloids were applied to a strong H for a long time. The deposition of nanoparticles may cause the colloids to attain an unstable state, which results in the disappearance of structural colors.

Reproducibility is a key challenge for the practical application of the photonics procedures. Fig. S2 illustrates the reflection spectra of the

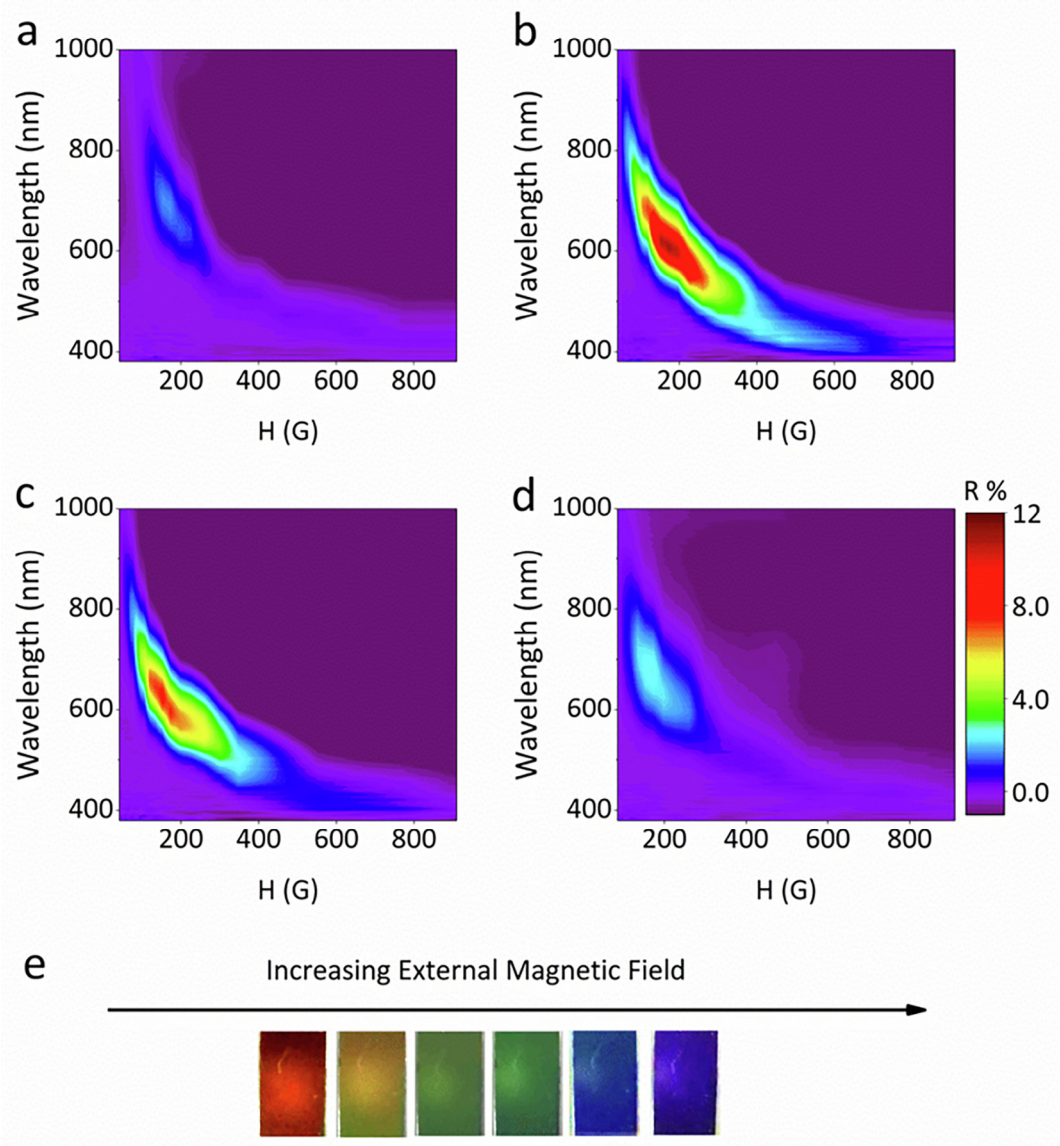

Fig. 5. Reflection spectra of superparamagnetic colloids at four different concentrations: (a) 20, (b) 10, (c) 5, and (d) 2.5 mg/mL. (e) A series of photographs of one as-prepared Fe_3O_4 colloid (10 mg/mL) encapsulated in a cuvette (the magnetic field increases from left to right).

samples after three washings with deionized water (Fig. S2a, b, and c correspond to washings 1, 2, and 3, respectively). After the additional washings, all reflection peaks demonstrated nearly no change. Fig. S3 displays the spectra of the samples after 3 and 7 days of store, and a slight decrease in reflectance intensities was noted. Because the citrate group and the Fe_3O_4 nanoparticle surface are covalently bonded, the resulting colloids have good chemical stability and respond to the magnetic field immediately. The aforementioned results clearly prove that the photonics procedures of superparamagnetic iron oxide nanoparticle are reproducible and can aid in creating photonic materials.

The diameter of the nanoparticles considerably influences the structural colors of the colloids. Fig. 4a–c shows the TEM images for particles with a diameter of 71, 100, and 135 nm. More than 200 nanoparticles were analyzed for each particle diameter. In general, the reflection peaks of small nanoparticles were at short wavelengths under a magnetic field. When the nanoparticle size was increased, the reflection peak was gradually red-shifted (Fig. 4d–f). The larger the particle size, the higher was the reflection intensity. In contrast to polyelectrolyte-capped Fe_3O_4 nanoparticles, citrate-capped nanoparticles without steric hindrance were assembled by a weak magnetic field [22]. A magnetic field higher than 40 G can drive nanoparticles when the magnetic packing forces overcome the electrostatic repulsive forces. As evident in Fig. 2c, the saturated magnetic moments of individual Fe_3O_4 nanoparticles exhibited an increasing trend when the nanoparticle size increased from 71 to 135 nm. Due to weak magnetic saturation moments, the assembly behavior of small-sized nanoparticles under the magnetic field was affected. There existed many defects in the photonic material, which resulted in the small nanoparticles having a low reflectivity under the magnetic field.

Fig. 5 shows the reflection spectra of colloids with a nanoparticle size of 100 nm at four different concentrations between 2.5 and 20 mg/mL. The structure of the formed tunable photonic material was in equilibrium with the magnetic packing forces and electrostatic repulsive forces. The citrate groups existing on the surface of Fe_3O_4 provided sufficient electrostatic repulsive force. The reflection intensity at low Fe_3O_4 concentrations was higher than that at high Fe_3O_4 concentrations (Fig. 5a) because of the decreased absorption at low concentrations. The saturation magnetization of the magnetic nanoparticle (size 100 nm) was 66.2 emu/g, which is considerably higher than that of a similar-sized nanoparticle synthesized using polyelectrolytes (approximately 45–60 emu/g) [19,22,23]. The nanoparticles had a high saturation magnetization in a low magnetic field (approximately

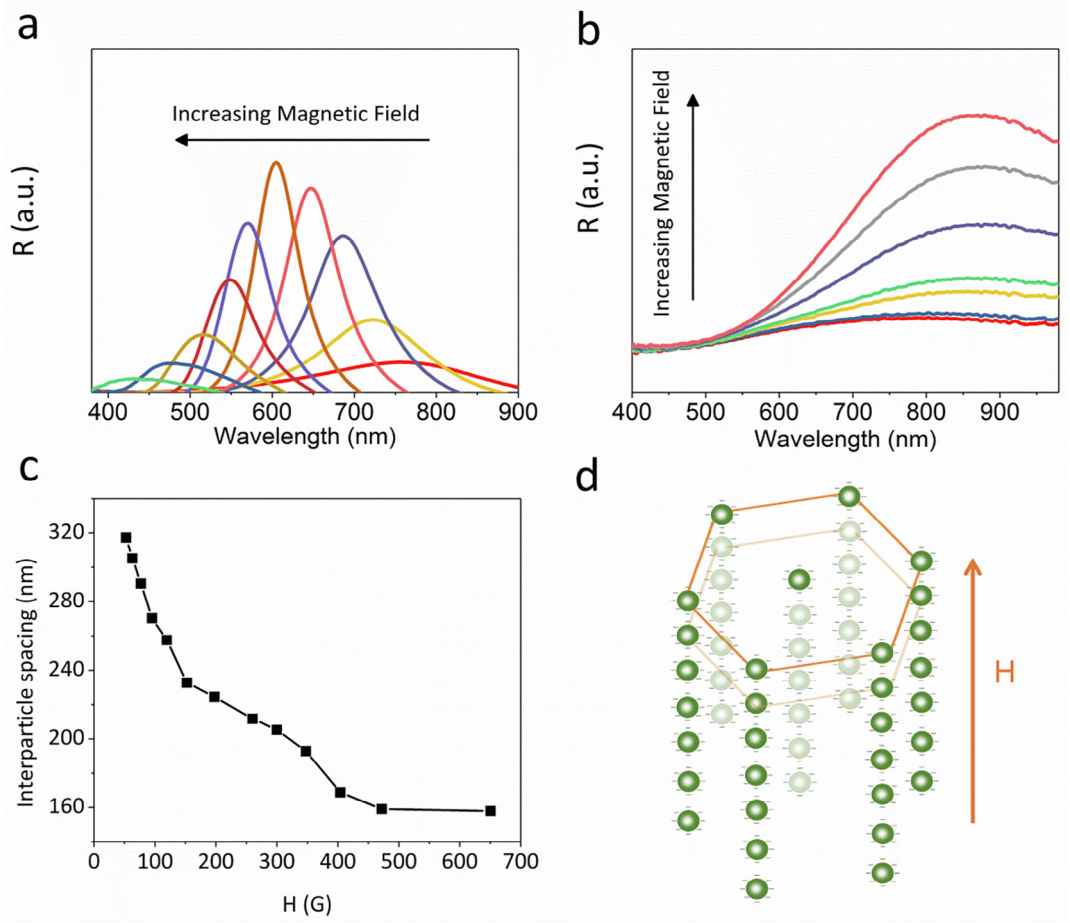

Fig. 6. Reflection peaks for the Fe_3O_4 colloid when the magnetic field is increased using an immersion probe in the (a) horizontal and (b) vertical directions. (c) Relation between the value of H and the estimated interparticle spacing along the direction of H. (d) Schematic of the assembly of iron oxide nanoparticles in the presence of an applied H.

30–300 G); however, the magnetic packing force was stronger than the electrostatic repulsive force at a high magnetic field. When H was higher than 800 G, the ordered structure was destroyed by the magnetic packing forces. As a result, the nanoparticles could not produce structural colors.

When the concentration of Fe_3O_4 decreased from 20 to 10 mg/mL (Fig. 5b), the reflection spectrum covered the entire visible range and the overall reflection intensity increased. Thus, the concentration influenced the reflection intensity. The dilution of Fe_3O_4 caused the citrate groups to ionize in aqueous solution, which enhanced the electrostatic repulsive interactions. A marginal change occurred in the reflection intensity and range when the Fe_3O_4 aqueous solution was diluted from 10 to 5 mg/mL (Fig. 5c), which indicated that certain concentration ranges had a small influence on the nanoparticle arrays of the Fe_3O_4 colloids under a magnetic field. The magnetic field strength required (30–600 G) for driving the nanoparticles to assembly was similar for all the four concentrations. After diluting the aqueous Fe_3O_4 solution from 5 to 2.5 mg/mL (Fig. 5d), the short-wavelength reflection faded away and the peak intensity decreased. If the concentration of colloids is decreased below 1.5 mg/mL after dilution, the visible reflection cannot be measured due to Brownian motion. The structural colors of Fe_3O_4 in aqueous solution changed from red to purple with a change in the magnetic field, as illustrated in the digital photographs (Fig. 5e). In general, small polyelectrolyte-capped Fe_3O_4 (60–100 nm) nanoparticles reflected only blue color in a weak H and had a saturation magnetization of less than 60 emu/g. Citrate-capped Fe_3O_4 had a smaller size (approximately 100 nm) and higher saturation magnetization (approximately 66 emu/g) than polyelectrolyte-capped Fe_3O_4 in a weak magnetic field.

As illustrated in Fig. S4, absorbance increased from 900 to 400 nm; this absorbance range is identical to the reflectance range of colloids with varying magnetic fields. As illustrated in Fig. 5b, when the H increases from 0 to 200 G, the number of layers in photonic materials increases. The reflectance peak has a blue shift from 800 to 600 nm, and the reflection intensity keeps growing. Moreover, at this stage, the effect of absorbance on the reflectance spectrum is not substantial. After the H exceeds 200 G, the reflection intensity is significantly influenced by the absorbance from Fe_3O_4. With the blue shift of the reflection peak, the effect of absorbance on the reflection intensity increases gradually. Consequently, the reflection intensity begins to decrease as H increases.

To further study the optical properties of the photonic material, the colloid was placed in a rectangular cuvette and one side of the cuvette was observed. The reflection spectra were obtained by applying parallel or perpendicular magnetic fields with different magnitudes. As depicted in Fig. 6a, the blue shift in the reflection peaks inside the colloids was consistent with the change in the reflection peaks outside the colloids. The reflection peaks exhibited a blue shift when H increased, whereas the interparticle distance of the nanoparticle arrays decreased. However, when the probe was perpendicular to the direction of the magnetic packing force, the position of the reflection peaks remained unchanged and the intensity of the peaks increased with an enhancement in the magnetic packing force (Fig. 6b). An increased number of ordered layers were formed perpendicular to the magnetic packing force. Therefore, the reflection intensity was enhanced. These results indicated that the reflection was mainly caused by the nanoparticles

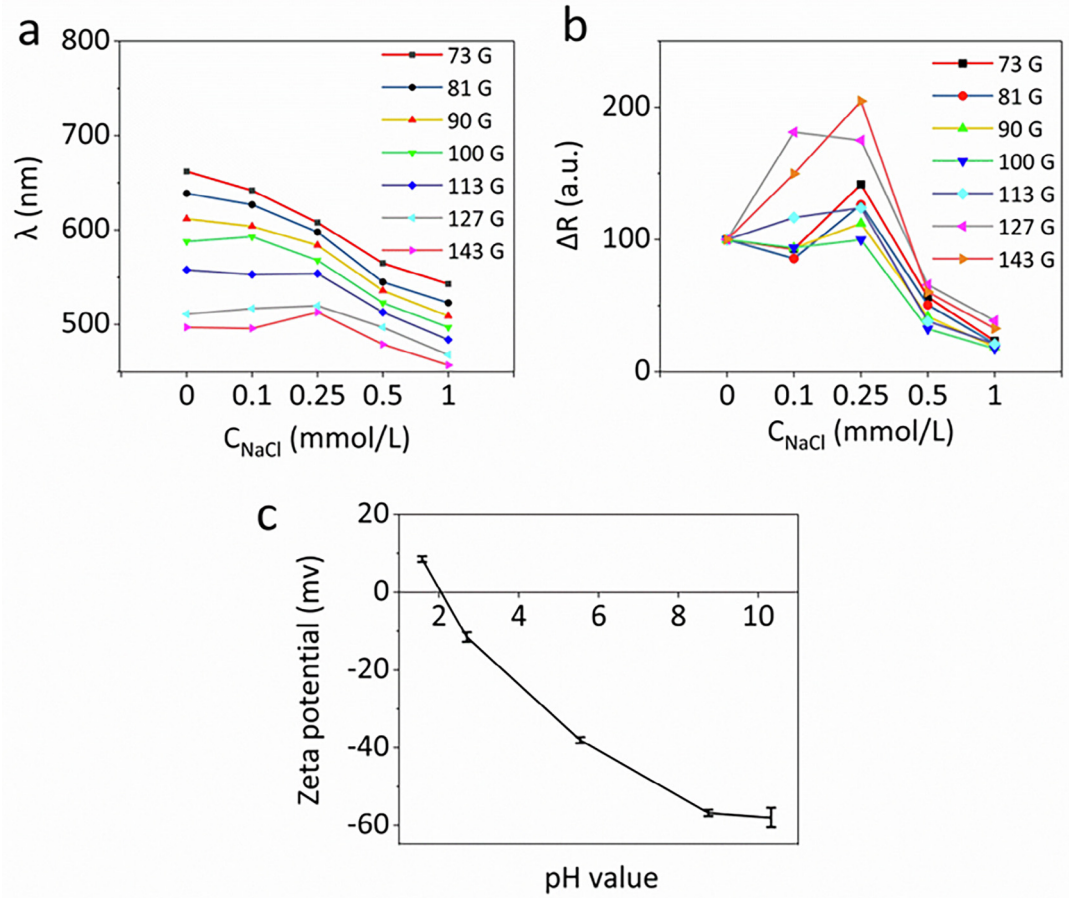

Fig. 7. Influence of the amount of electrolyte NaCl on the (a) wavelength (λ) and (b) relative intensity (ΔR) of the reflection. (c) Zeta potential of Fe_3O_4 colloids with different pH values. (d) Influence of the pH value on the main wavelength and relative wavelength of the colloids.

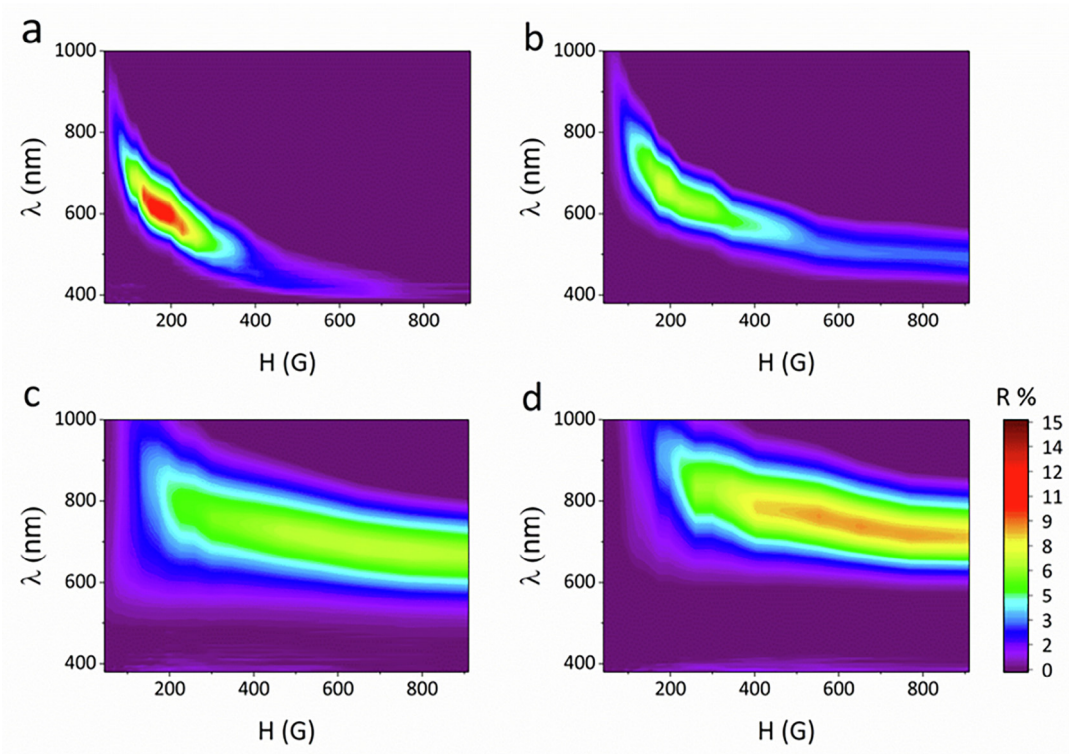

Fig. 8. Reflection spectra of the core–shell nanoparticle colloids with the same Fe_3O_4 core diameter (100 nm) and different shell thicknesses: (a) 0, (b) 10, (c) 25, and (d) 50 nm.

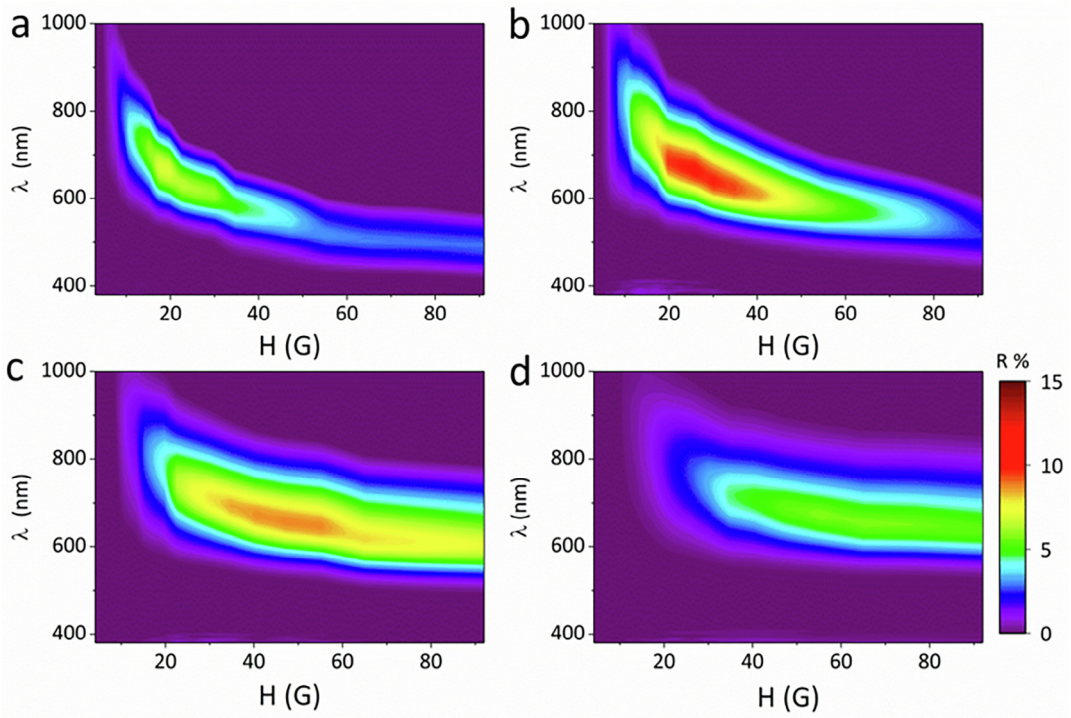

Fig. 9. Reflection spectra of as-obtained Fe_3O_4@SiO_2 colloids at concentrations of 40, 20, 10, and 1 mg/mL.

assemblies. The lattice plane spacing (d) of the particle arrays was estimated using Bragg's law [54], which is given as follows: $d = \lambda / 2n\sin\theta$, where λ is the reflection wavelength, n is the refractive index of the colloid, and $\theta = 90^\circ$ is the Bragg angle. The interparticle spacing (d′) can be obtained by subtracting the nanoparticle diameter from d. The interparticle spacing decreased as H increased (Fig. 6c). The Fe_3O_4 colloid was structurally anisotropic (Fig. 6d). Therefore, it exhibited nanoparticle arrays of three-dimensional structures.

The Fe_3O_4 nanoparticles modified with sodium citrate had good chemical stability in aqueous solution. The amount of electrolyte (such as NaCl) influenced the structural colors of the colloids. Fig. 7 displays the change in λ and ΔR (relative intensity) of the reflection for Fe_3O_4 colloids with different NaCl concentrations (0–1 mmol/L) at seven magnetic field intensities. In general, an increase in the amount of NaCl resulted in a decrease in the electrostatic repulsive force of polyelectrolyte-capped Fe_3O_4 because the counterions provided strong Debye screening in a double layer on the surface of the nanoparticles [55]. However, the peak shift of the Fe_3O_4 colloids decreased slowly at low ionic strength under a applied H. The influence of the amount of NaCl on the relative intensity of the reflection is shown in Fig. 7b. The highest ΔR value is observed when a balance is achieved between the magnetic packing forces and electrostatic repulsive forces. Under a strong external field (120–150 G), the reflection had a high relative intensity at a low NaCl amount and the increase in the packing forces countered the decrease in the electrostatic repulsive forces. An increase in the electrolyte amount weakened the interparticle electrostatic repulsive force. When the electrostatic repulsive forces weakened, the nanoparticle arrays became disordered. When the electrolyte concentration increased, the relative intensity of the reflection steadily decreased. For colloids under a weak external field, the weak electrostatic force produced at a certain nonzero NaCl amount can be countered by a magnetic packing force of the appropriate magnitude. In our system, the relative intensity of the reflection first increased with an increase in the NaCl amount. The highest intensity was obtained at $C_{NaCl} = 0.25$ mmol/L. The relative intensity decreased at NaCl concentrations higher than 0.25 mmol/L because the electrostatic repulsive force could not counter the magnetic packing force for building ordered particle arrays [56,57]. Fig. 7c shows the zeta potential of the colloid, which was measured at pH values of approximately 1–12. The isoelectric point of the synthesized colloid was observed at the pH value of 2. When the pH value increased from 1.58 to 10.32, the negative surface charge of the nanoparticles increased. With an increase in the pH value, an increasing number of citrate groups adsorbed at Fe_3O_4 were gradually ionized, which resulted in an increase in the zeta potential. The aforementioned results indicate that the citrate-capped Fe_3O_4 nanoparticles had a more stable performance than the polyelectrolyte-capped Fe_3O_4 nanoparticles.

After various sizes of SiO_2 layers were coated on the Fe_3O_4 nanoparticles, the Fe_3O_4@SiO_2 core–shell nanoparticles dispersed in deionized H_2O formed photonic materials under an applied H, showing the similar optical characteristics of Fe_3O_4 colloids. The reflection peak of the superparamagnetic Fe_3O_4@SiO_2 colloids were measured under an external field for nanoparticles with the same core diameter (100 nm) and four shell thicknesses (0, 10, 25, and 50 nm). The reflection peak red shifted to long wavelengths when the silicon dioxide layer increased. The controlled range of the reflection wavelength for the 114 nm nanoparticle (100 nm core and 10 nm shell) was 420–800 nm (Fig. 8a). The reflection wavelength of the Fe_3O_4@SiO_2 colloids exhibited a red shift with respect to the reflection wavelength of the Fe_3O_4 colloids at the same concentration (Fig. 8b). Moreover, the reflection intensity of the Fe_3O_4@SiO_2 colloids was lower than that of the Fe_3O_4 colloids. The reflection intensity for the Fe_3O_4@SiO_2 colloids continued to increase with increasing H until a stable value was reached. However, a further increase in H only caused marginal changes in the reflection peak and reflection intensity. Because of the Derjaguin–Landau–Verwey–Overbeek theory, when the electrostatic repulsive force from the highly charged Fe_3O_4@SiO_2 nanoparticles balances the magnetic packing force, ordered structures are formed [49,58,59]. Controlling the size of the core and shell allows the reflection of a fixed wavelength under a certain magnetic field range. Due to the thick SiO_2 layers and periodicity, the wavelength of the controlled reflection covered the near–infrared–red range for nanoparticle with a average diameter of 150 nm (100 nm core and 25 nm shell) and 200 nm (100 nm core and 50 nm shell) under a magnetic field

(Fig. 8c,d).

Similar to the Fe_3O_4 colloids, the core–shell colloids also exhibited a trend where the reflection intensities first increased and then decreased under a applied H. Fig. 9 shows the reflection spectra of the Fe_3O_4@SiO_2 colloids (100 nm core and 10 nm shell) at concentrations of 40, 20, 10, and 1 mg/mL. The concentration of the Fe_3O_4@SiO_2 colloids influenced the reflection intensity and range of the reflection peak. The SiO_2 shell coating improved the uniformity of the nanoparticles. Therefore, the Fe_3O_4@SiO_2 colloids exhibited a higher reflection intensity than the Fe_3O_4 colloids at the same concentration. Furthermore, the electrostatic repulsive force had a considerable influence on the reflection properties of the Fe_3O_4 colloids, whereas the solvation force mainly influenced the reflection properties of the Fe_3O_4@SiO_2 colloids. Fe_3O_4@SiO_2 exhibited structural color even at a concentration of 1 mg/mL; however, Fe_3O_4 suspension could not exhibit structural color at the same concentration.

Conclusions

In summary, Fe_3O_4 nanoparticles with citrate groups as a capping agent can be used to form stable colloids by dispersed in aqueous solution. The nanoparticles assemble themselves into an ordered nanostructure when balance is achieved between the electrostatic repulsive forces and magnetic packing forces. Fe_3O_4 colloids exhibit tunable structural colors under a magnetic field ranging from 20 to 800 G and can be used as building blocks of tunable photonic materials. Their reflection spectra have a wavelength range of approximately 420–800 nm, which includes the entire visible range. The amount of stray electrolytes considerably affects the structural color of the colloids because it changes the strength of the electrostatic repulsive force. The nanoparticle diameter, nanoparticle concentration, and shell thickness of the core–shell nanoparticles affect the reflection intensity and spectral range. The long-range order in nanostructures is only influenced by the direction of the applied H when colloidal nanoparticle arrays are built for visible wavelengths. The reflection peak shifts to long wavelengths and covers the near-infrared region up to 980 nm when the shell thickness of Fe_3O_4@SiO_2 increases. The above properties of superparamagnetic nanoparticles are promising candidates for achieving full-color display, and they also help in understanding the mechanism of photonic materials.

Acknowledgements

This project was supported by the National Natural Science Foundation of China (Grant No. 61775242), the Key Program of Natural Science Foundation of China (No. 61835013), Guangzhou Municipal Science and Technology Bureau, China (Grant No. 201804020031) and Guangdong Science and Technology Department, China (Grant No. 2014A010106009).

Appendix A. Supplementary material

Supplementary data to this article can be found online at https://doi.org/10.1016/j.rinp.2019.102366.

References

[1] Park H, Schadt MJ, Wang L, Lim IS, Njoki PN. Fabrication of magnetic Core@Shell Fe Oxide@Au nanoparticles for interfacial bioactivity and bio-separation. Langmuir 2007;23:9050–6.
[2] Elingarami S, Zeng X. A short review on current use of magnetic nanoparticles for bio-separation, sequencing, diagnosis and drug delivery. Adv Sci Lett 2011;4:3295–300.
[3] Albert EL, Che Abdullah CA, Shiroshaki Y. Synthesis and characterization of graphene oxide functionalized with magnetic nanoparticle via simple emulsion method. Results Phys 2018;11:944–50.
[4] Shang L, Liang Y, Li M, et al. "Naked" magnetically recyclable mesoporous Au-γ-Fe_2O_3 nanocrystal clusters: a highly integrated catalyst system. Adv Funct Mater 2017;27:1606215.
[5] Purbia R, Paria S. Noble metals decorated hierarchical maghemite magnetic tubes as an efficient recyclable catalyst. J Colloid Interf Sci 2018;511:463–73.
[6] Ruíz-Baltazar ÁDJ, Reyes-López SY, Mondragón-Sánchez MDL, Robles-Cortés AI, Pérez R. Eco-friendly synthesis of Fe_3O_4 nanoparticles: evaluation of their catalytic activity in methylene blue degradation by kinetic adsorption models. Results Phys 2019;12:989–95.
[7] Wang W, Fan X, Li F, et al. Magnetochromic photonic hydrogel for an alternating magnetic field-responsive color display. Adv Opt Mater 2018;6:1701093.
[8] Lee I, Kim D, Kal J, et al. Quasi-amorphous colloidal structures for electrically tunable full-color photonic pixels with angle-independency. Adv Mater 2010;22:4973–7.
[9] Ge J, Goebl J, He L, Lu Z, Yin Y. Rewritable photonic paper with hygroscopic salt solution as ink. Adv Mater 2009;21:4259–64.
[10] Yan D, Zhu X, Mao Y, et al. Hierarchically organized CNT@TiO_2@Mn_3O_4 nanostructures for enhanced lithium storage performance. J Mater Chem A 2017;5:17048–55.
[11] Wu JH, Ko SP, Liu HL, Kim S, Ju JS, Kim YK. Sub 5nm magnetite nanoparticles: Synthesis, microstructure, and magnetic properties. Mater Lett 2007;61:3124–9.
[12] Lin C, Ho J. Structural analysis and catalytic activity of Fe_3O_4 nanoparticles prepared by a facile co-precipitation method in a rotating packed bed. Ceram Int 2014;40:10275–82.
[13] Liu Y, Liu P, Su Z, Li F, Wen F. Attapulgite–Fe_3O_4 magnetic nanoparticles via co-precipitation technique. Appl Surf Sci 2008;255:2020–5.
[14] Eom Y, Abbas M, Noh HY, Kim CG. Morphology-controlled synthesis of highly crystalline Fe_3O_4 and $CoFe_2O_4$ nanoparticles using a facile thermal decomposition method. Rsc Adv 2016;6:15861–7.
[15] Peng S, Sun S. Synthesis and characterization of monodisperse hollow Fe_3O_4 nanoparticles. Angew Chem Int Ed 2007;46:4155–8.
[16] Li Z, Sun Q, Gao M. Preparation of water-soluble magnetite nanocrystals from hydrated ferric salts in 2-pyrrolidone: mechanism leading to Fe_3O_4. Angew Chem Int Ed 2005;44:123–6.
[17] Deng Y, Cai Y, Sun Z, et al. Multifunctional mesoporous composite microspheres with well-designed nanostructure: a highly integrated catalyst system. J Am Chem Soc 2010;132:8466–73.
[18] Wang W, Zhuang L, Zhang Y, Shen H. Synthesis of monodisperse MFe_2O_4 (M = Fe and Zn) nanoparticles for polydiethylsiloxane-based ferrofluid with a solvothermal method. Mater Res Bull 2015;69:61–4.
[19] Ma M, Zhang Q, Dou J, et al. Fabrication of one-dimensional Fe_3O_4/P(GMA–DVB) nanochains by magnetic-field-induced precipitation polymerization. J Colloid Interf Sci 2012;374:339–44.
[20] Ge J, Hu Y, Zhang T, Yin Y. Superparamagnetic composite colloids with anisotropic structures. J Am Chem Soc 2007;129:8974–5.
[21] Ge J, Hu Y, Biasini M, Beyermann WP, Yin Y. Superparamagnetic magnetite colloidal nanocrystal clusters. Angew Chem 2007;46:4342–5.
[22] Sheng Y, Xue J. Synthesis and properties of Au–Fe_3O_4 heterostructured nanoparticles. J Colloid Interf Sci 2012;374:96–101.
[23] Ko KH, Park E, Lee H, Lee W. Low-power all-organic electrophoretic display using self-assembled charged poly(t-butyl methacrylate) microspheres in isoparaffinic fluid. Acs Appl Mater Inter 2018;10:11776–84.
[24] Lee SY, Choi J, Jeong J, Shin JH, Kim S. Magnetoresponsive photonic microspheres with structural color gradient. Adv Mater 2017;29:1605450.
[25] Zhang Y, Fu Q, Ge J. Photonic sensing of organic solvents through geometric study of dynamic reflection spectrum. Nat Commun 2015;6:7510.
[26] Zheng L, Cheng H, Liang F, et al. Porous TiO_2 photonic band gap materials by anodization. J Phys Chem C 2012;116:5509–15.
[27] Zhang R, Zeng F, Pang F, Ge J. Substantial enhancement toward the photocatalytic activity of CdS quantum dots by photonic crystal-supporting films. Acs Appl Mater Inter 2018;10:42241–8.
[28] Xiao M, Li Y, Zhao J, et al. Stimuli-responsive structurally colored films from bioinspired synthetic melanin nanoparticles. Chem Mater 2016;28:5516–21.
[29] Li Y, Zhou L, Liu G, Chai L, Fan Q, Shao J. Study on the fabrication of composite photonic crystals with high structural stability by co-sedimentation self-assembly on fabric substrates. Appl Surf Sci 2018;444:145–53.
[30] Ge J, Yin Y. Magnetically responsive colloidal photonic crystals. J Mater Chem 2008;18:5041.
[31] Luo W, Ma H, Mou F, Zhu M, Yan J, Guan J. Steric-repulsion-based magnetically responsive photonic crystals. Adv Mater 2014;26:1058–64.
[32] Xu X, Friedman G, Humfeld KD, Majetich SA, Asher SA. Superparamagnetic photonic crystals. Adv Mater 2001; 22: 1681.
[33] Li W, Wu H. Sodium citrate functionalized reusable Fe_3O_4@TiO_2 photocatalyst for water purification. Chem Phys Lett 2017;686:178–82.
[34] Dikhtiarenko A, Khainakov SA, García JR, et al. Hydrothermal synthesis and physicochemical properties of ruthenium(0) nanoparticles. J Alloy Compd 2012;536:S437–40.
[35] Kochkar H, Aouine M, Ghorbel A, Berhault G. Shape-controlled synthesis of silver and palladium nanoparticles using β-cyclodextrin. J Phys Chem C 2011;115:11364–73.
[36] Piella J, Bastús NG, Puntes V. Size-controlled synthesis of sub-10-nanometer citrate-stabilized gold nanoparticles and related optical properties. Chem Mater 2016;61:3124–9.
[37] Cheng C, Wen Y, Xu X, Gu H. Tunable synthesis of carboxyl-functionalized magnetite nanocrystal clusters with uniform size. J Mater Chem 2009;19:8782–8.
[38] Dong F, Guo W, Bae J, Kim S, Ha C. Highly porous, water-soluble, superparamagnetic, and biocompatible magnetite nanocrystal clusters for targeted drug delivery. Chem Eur J 2011;17:12802–8.

[39] Tan J, Jin X. Monodisperse, colloidal and luminescent calcium fluoride nanoparticles via a citrate-assisted hydrothermal route. J Colloid Interf Sci 2018;531:444–50.
[40] Rosapardo I, Roigpons M, Heredia AA, et al. Fe_3O_4@Au@mSiO_2 as an enhancing nanoplatform for Rose Bengal photodynamic activity. Nanoscale 2017.
[41] Lee H, Kim S, Lee H, Park KH, Kim Y, Yi G. Highly stable electrical manipulation of reflective colors in colloidal crystals of sulfate iron oxide particles in organic media. Rsc Adv 2016;6:100167–73.
[42] Wang F, Li M, Yu L, et al. Corn-like recoverable γ-Fe_2O_3@SiO_2@TiO_2 photocatalyst induced by magnetic dipole interactions. Sci Rep 2017:7.
[43] Bhargava G, Gouzman I, Chun CM, Ramanarayanan TA, Bernasek SL. Characterization of the "native" surface thin film on pure polycrystalline iron: a high resolution XPS and TEM study. Appl Surf Sci 2007;253:4322–9.
[44] Zhang W, Chen J, Wang W, et al. Ultrasonic assisted rapid synthesis of high uniform super-paramagnetic microspheres with core-shell structure and robust magneto-chromatic ability. J Magn Magn Mater 2017;426:1–10.
[45] Liu M, Cai C, Li J, Zhao J, Teng W, Liu R. Stöber synthesis of tannic acid–-formaldehyde resin polymer spheres and their derived carbon nanospheres and nanocomposites for oxygen reduction reaction. J Colloid Interf Sci 2018;528:1–9.
[46] Wilson D, Langell MA. XPS analysis of oleylamine/oleic acid capped Fe3O4 nanoparticles as a function of temperature. Appl Surf Sci 2014;303:6–13.
[47] Gao J, Ran X, Shi C, Cheng H, Cheng T, Su Y. One-step solvothermal synthesis of highly water-soluble, negatively charged superparamagnetic Fe_3O_4 colloidal nanocrystal clusters. Nanoscale 2013;5:7026.
[48] Yang P, Li H, Zhang S, et al. Gram-scale synthesis of superparamagnetic Fe_3O_4 nanocrystal clusters with long-term charge stability for highly stable magnetically responsive photonic crystals. Nanoscale 2016;8:19036.
[49] Xu X, Friedman G, Humfeld KD, Majetich SA, Asher SA. Synthesis and utilization of monodisperse superparamagnetic colloidal particles for magnetically controllable photonic crystals. Chem Mater 2002;14:1249–56.
[50] Bibette J. Monodisperse ferrofluid emulsions. J Magn Magn Mater 1993;122.
[51] Zhao Y, Ying Y, Wang Q, Hu H. Simulation on microstructure and optical property of magnetic fluid photonic crystal. IEEE T Magn 2014;50:1–12.
[52] Pal A, Malik V, He L, et al. Tuning the colloidal crystal structure of magnetic particles by external field. Angew Chem Int Ed 2015;54:1803–7.
[53] Shen H, Wang Z, Wu Y, Yang B. One-dimensional photonic crystals: fabrication, responsiveness and emerging applications in 3D construction. Rsc Adv 2016;6:452–5.
[54] Ge J, Hu Y, Yin Y. Highly tunable superparamagnetic colloidal photonic crystals. Angew Chem Int Ed 2007;46:7428–31.
[55] Lobaskin V, Dunweg B, Medebach M, Palberg T, Holm C. Electrophoresis of colloidal dispersions in the low-salt regime. Phys Rev Lett 2007;98:176105.
[56] Ge J, Hu Y, Zhang T, Huynh T, Yin Y. Self-assembly and field-responsive optical diffractions of superparamagnetic colloids. Langmuir 2008;24:3671–80.
[57] Xu X, Friedman G, Humfeld KD, Majetich SA, Asher SA. Superparamagnetic photonic crystals. Adv Mater 2001;22:1681–4.
[58] Ma H, Tang K, Luo W, Ma L, Cui Q. Photonic nanorods with magnetic responsiveness regulated by lattice defects. Nanoscale 2017:3105–13.
[59] He L, Wang M, Ge J, Yin Y. Magnetic assembly route to colloidal responsive photonic nanostructures. Account Chem Res 2012;45:1431–40.